
Learning for Dynamic Combinatorial Optimization without Training Data

Yiqiao Liao
UC San Diego
yil345@ucsd.edu

Farinaz Koushanfar
UC San Diego
fkoushanfar@ucsd.edu

Parinaz Naghizadeh
UC San Diego
parinaz@ucsd.edu

Abstract

We introduce DyCO-GNN, a novel unsupervised learning framework for Dynamic Combinatorial Optimization that requires no training data beyond the problem instance itself. DyCO-GNN leverages structural similarities across time-evolving graph snapshots to accelerate optimization while maintaining solution quality. We evaluate DyCO-GNN on dynamic maximum cut, maximum independent set, and the traveling salesman problem across diverse datasets of varying sizes, demonstrating its superior performance under tight and moderate time budgets. DyCO-GNN consistently outperforms the baseline methods, achieving high-quality solutions up to 3–60x faster, highlighting its practical effectiveness in rapidly evolving resource-constrained settings.

1 Introduction

Combinatorial optimization (CO) lies at the heart of many critical scientific and industrial problems [37]. Since most CO problems are NP-hard, solving large-scale instances is computationally prohibitive. Traditionally, solving such problems has relied on exact solvers, heuristics, and meta-heuristics, whose design requires problem-specific insights. Recent advances in machine learning, particularly graph neural networks (GNNs), have opened new avenues for learning heuristics in a data-driven manner [6, 10, 18, 23–26]. GNNs have emerged as a powerful framework for learning over relational and structured data [7, 15, 28, 49], with an inductive bias particularly suited for representing the underlying graph structures inherent in many CO problems.

Most existing approaches applying machine learning to CO are learning-heavy, requiring training on a large set of problem instances to learn *heuristics that generalize* to test instances. Training can take hours or even days on multiple GPUs [33, 51]. Schuetz et al. [42] started another line of research that aims to develop an unsupervised learning (UL) method that learns *instance-specific heuristics*. Their method, PI-GNN, directly applies a GNN to the problem instance of interest and optimizes a CO objective. Under this design, no explicit “training” is involved; the runtime is the time it takes for the model to converge on each problem instance. Prior work has shown that problems such as maximum cut (MaxCut) and maximum independent set (MIS) on graphs with thousands of nodes can be solved by PI-GNN-based methods in minutes [17, 19]. We provide further runtime analysis in Section 5.

While significant progress has been made in learning for static CO, many real-world problems are inherently dynamic, involving inputs or constraints that evolve over time [53, 55]. In such settings, decisions must be updated continually, and practical algorithms must be efficient. A simple approach is to treat each snapshot of the problem instance as a static problem and solve it from scratch. However, significant overlap often exists in the node and edge sets across snapshots. Leveraging information from previous snapshots can improve both runtime and solution quality. For example, in MaxCut, the previous solution might serve as a good starting point after edge additions.

In this paper, we focus on learning for dynamic combinatorial optimization (DCO) and aim to advance the PI-GNN line of research. We present DyCO-GNN for DCO. To the best of our knowledge, our work is the first to apply machine learning to DCO problems. Our main contributions are as follows.

- We propose DyCO-GNN, a general UL-based optimization method for DCO that requires *no training data* except the problem instance of interest.
- We empirically validate the applicability of DyCO-GNN to various CO problems under dynamic settings, including MaxCut, MIS, and the traveling salesman problem (TSP).
- We demonstrate that DyCO-GNN achieves superior solution quality when the time budget is limited and outperforms the static counterpart with up to **3–60x** speedup.

2 Related work

Machine learning for static CO has predominantly relied on supervised learning approaches [10, 18, 23, 24, 32, 33, 44, 50]. These methods train models to predict high-quality solutions given a large dataset of problem instances paired with optimal or near-optimal labels. However, generating such labels is computationally expensive, especially for large-scale instances, making these methods less practical for many real-world applications.

To address this limitation, UL and reinforcement learning (RL) approaches have emerged as promising alternatives [6, 25, 26, 29, 39, 41, 47, 48, 51]. These methods aim to learn optimization strategies directly from instance structures or reward signals without requiring labeled data. While they alleviate the need for ground-truth solutions, most UL and RL-based techniques still involve extensive offline training over large datasets to develop *heuristics that generalize*. Training such models can be time-consuming, often requiring hours or days on high-performance hardware [33, 51].

A different paradigm was introduced by Schuetz et al. [42], who proposed PI-GNN—an unsupervised framework that learns *instance-specific heuristics* by directly optimizing the CO objective on a single instance. This avoids any offline training and allows the method to be tailored to each problem instance during inference. PI-GNN combines a learnable embedding layer with a GNN and has been shown to achieve competitive performance across tasks such as MaxCut and MIS. Subsequent works have improved its solution quality and extended its design to incorporate higher-order relational reasoning [17, 19], achieving strong results even on large-scale graph instances.

Despite advances in instance-specific optimization, existing efforts have focused exclusively on static CO. The challenge of adapting learned heuristics efficiently to dynamic settings remains, to our knowledge, unexplored. Our work builds upon the PI-GNN line of research to propose new methods for DCO, where we aim to reuse and adapt learned solutions across temporally evolving problem instances without requiring optimization from scratch. We review the optimization theory literature on DCO, which is complementary to our learning-based approach, in Appendix A.

3 Preliminaries

3.1 Static CO: PI-GNN and quadratic binary unconstrained optimization (QUBO)

Consider a graph $G_p = (V_p, E_p, w_p)$ with node set $V_p = \{1, 2, \dots, n_p\}$, edge set E_p , and edge weights w_p representing or inherent in a CO problem instance p . PI-GNN is a general UL framework for static CO problems based on QUBO [8, 12, 34]. A QUBO problem is defined by:

$$\min_x \ell(x; Q_p) = x^T Q_p x = \sum_{i=1}^N \sum_{j=1}^N Q_{ij} x_i x_j, \quad (1)$$

where $x \in \{0, 1\}^N$ is a binary vector with N components, and $Q_p \in \mathbb{R}^{N \times N}$ is a symmetric matrix encoding the cost coefficients, obtained based on the graph G_p . There are no explicit constraints, with all constraints incorporated implicitly via the structure of the Q matrix. Many CO problems, such as MaxCut, MIS, and TSP, can be reformulated as QUBO instances, making it a universal encoding framework for a wide class of problems. For a given static CO problem instance, PI-GNN learns to find a solution via $\mathcal{A}(G_p; \theta)$, where θ is the set of learnable parameters. Since the input graph has no node features, PI-GNN randomly initializes learnable embeddings for the nodes and feeds them to a

GNN. It then optimizes a differentiable QUBO objective in the form of Equation 1 by outputting a relaxed solution (i.e., $x \in [0, 1]^n$) followed by a final rounding step to obtain valid binary solutions.

MaxCut. Without loss of generality, we assume the edges have unit weights. The goal of MaxCut is to find a partition of the nodes into two disjoint subsets that maximizes the number of edges between them. We can model MaxCut solutions using $x \in \{0, 1\}^n$ where $x_i = 0$ if node i is in one set, and $x_i = 1$ if node i is in the other set. The objective can be formulated as $\sum_{(i,j) \in E} (2x_i x_j - x_i - x_j)$, which is an instance of QUBO [12].

MIS. MIS is the largest subset of non-adjacent nodes. Similar to MaxCut, we let $x_i = 1$ if node i is in the independent set and $x_i = 0$ otherwise. The objective can be formulated as $-\sum_{i \in V} x_i + M \sum_{(i,j) \in E} x_i x_j$, where $M \in \mathbb{R}_{>0}$ is a penalty term enforcing the independent set constraint [8].

TSP. We consider symmetric TSP instances modeled as undirected complete graphs. TSP aims to find the route that visits each node exactly once and returns to the origin node with the lowest total distance traveled. In contrast to MaxCut and MIS, we use a binary matrix $X \in \{0, 1\}^{n \times n}$ to represent a route where $X_{ij} = 1$ denotes visiting node i at step j . Following [20, 34], we adopt the following objective: $\sum_{(i,j) \in E} w_{ij} \sum_{v=1}^n X_{iv} X_{j(v+1)} + M \sum_{i=1}^n (1 - \sum_{j=1}^n X_{ij})^2 + M \sum_{j=1}^n (1 - \sum_{i=1}^n X_{ij})^2$, where w_{ij} is the distance between node i and node j , $X_{j(n+1)} = X_{j1}$, accounting for the requirement of returning to the origin node, and $M \in \mathbb{R}_{>0}$ is a penalty term to ensure X represents a valid route. During the QUBO objective computation, we simply flatten X to an n^2 -dimensional vector.

3.2 DCO on graphs

We focus on DCO problems on discrete-time dynamic graphs (DTDGs). A DTDG representing a DCO instance is a sequence $[G_p^{(1)}, G_p^{(2)}, \dots, G_p^{(T)}]$ of graph snapshots where each $G_p^{(t)} = (V_p^{(t)}, E_p^{(t)}, w_p^{(t)})$ has a node set $V_p^{(t)} = \{1, 2, \dots, n_p^{(t)}\}$, an edge set $E_p^{(t)}$, and edge weights $w_p^{(t)}$. For dynamic MaxCut and MIS, we consider the scenario where the node set $V_p^{(t)}$ and edge set $E_p^{(t)}$ change over time, and $w_p^{(t)} = 1$ for all $t \in \{1, 2, \dots, T\}$. For dynamic TSP, we consider the case where one of the nodes moves along a trajectory. Effectively, $V_p^{(1)} = V_p^{(2)} = \dots = V_p^{(T)}$ and $E_p^{(1)} = E_p^{(2)} = \dots = E_p^{(T)}$, but $w_p^{(t)}$ varies for each t .

Let $\Omega_p^{(t)}$ denote the set of discrete feasible solutions for snapshot $G_p^{(t)}$. For MaxCut and MIS, $\Omega_p^{(t)}$ is a subset of $\{0, 1\}^{n_p^{(t)}}$. For TSP, $\Omega_p^{(t)}$ is the set of all possible routes that visit each node exactly once and return to the origin node. The objective is to find the optimal solution for each snapshot of a given DCO problem instance: $x^{(t)*} = \operatorname{argmin}_{x \in \Omega_p^{(t)}} \ell(x; Q_p^{(t)})$, where $\ell(\cdot; Q_p^{(t)})$ denotes the cost function as defined earlier for each snapshot. For evaluation, we compute the mean approximation ratio (ApR) across all snapshots: Mean ApR = $\frac{1}{T} \sum_{t=1}^T \ell(x^{(t)}; Q_p^{(t)}) / \ell(x^{(t)*}; Q_p^{(t)})$.

4 Method

4.1 Warm-starting PI-GNN

Given a sequence of graph snapshots $[G_p^{(1)}, G_p^{(2)}, \dots, G_p^{(T)}]$, PI-GNN independently initiates an optimization process for each snapshot. One potential issue is that the time interval between two consecutive snapshots may be shorter than the convergence time of PI-GNN. In such cases, faster convergence is required. Considering the structural similarity across snapshots, a straightforward baseline method is to warm start the optimization using the parameters from the previous snapshot. Effectively, the “solution” to the previous snapshot serves as the initialization for the current one, allowing the model to “fine-tune” the solution instead of optimizing everything from scratch. We detail the procedure of warm-starting PI-GNN under different time budgets in Algorithm 1.

Limitations of naive warm start. Upon empirical evaluation, naively warm-starting PI-GNN exhibits several limitations. Figure 1 compares the performance of warm-started and static PI-GNN on dynamic MaxCut and MIS instances. Most notably, we observe that while warm start can potentially outperform static PI-GNN under a stringent time constraint, its advantages diminish quickly as the time budget increases. Specifically, when the time constraint is relaxed, warm-started models tend to produce lower-quality solutions than their static counterparts. Although warm start does accelerate convergence, the results it converges to are generally suboptimal.

Algorithm 1 Warm-starting PI-GNN

Require:

 Problem instance: $[G_p^{(1)}, G_p^{(2)}, \dots, G_p^{(T)}]$
 Max epochs for convergence: epoch_{\max}
 Epochs for warm start optimization: epoch_{ws}

- 1: Randomly initialize $\theta^{(1)}$
 - 2: Construct $[Q_p^{(1)}, Q_p^{(2)}, \dots, Q_p^{(T)}]$
for $[G_p^{(1)}, G_p^{(2)}, \dots, G_p^{(T)}]$
 - 3: **for** $i = 1$ to epoch_{\max} **do**
 - 4: Predict $x^{(1)}$ via $\mathcal{A}(G_p^{(1)}; \theta^{(1)})$
 - 5: Update $\theta^{(1)}$ using $\nabla \ell(x^{(1)}; Q_p^{(1)})$
 - 6: **end for**
 - 7: **for** $t = 2$ to T **do**
 - 8: $\theta^{(t)} \leftarrow \theta^{(t-1)}$
 - 9: **for** $i = 1$ to epoch_{ws} **do**
 - 10: Predict $x^{(t)}$ via $\mathcal{A}(G_p^{(t)}; \theta^{(t)})$
 - 11: Update $\theta^{(t)}$ using $\nabla \ell(x^{(t)}; Q_p^{(t)})$
 - 12: **end for**
 - 13: **end for**
-

Algorithm 2 DyCO-GNN

Require:

 Problem instance: $[G_p^{(1)}, G_p^{(2)}, \dots, G_p^{(T)}]$
 Max epochs for convergence: epoch_{\max}
 Epochs for warm start optimization: epoch_{ws}
 SP parameters: λ_{shrink} and λ_{perturb}

- 1: Randomly initialize $\theta^{(1)}$
 - 2: Construct $[Q_p^{(1)}, Q_p^{(2)}, \dots, Q_p^{(T)}]$
for $[G_p^{(1)}, G_p^{(2)}, \dots, G_p^{(T)}]$
 - 3: **for** $i = 1$ to epoch_{\max} **do**
 - 4: Predict $x^{(1)}$ via $\mathcal{A}(G_p^{(1)}; \theta^{(1)})$
 - 5: Update $\theta^{(1)}$ using $\nabla \ell(x^{(1)}; Q_p^{(1)})$
 - 6: **end for**
 - 7: **for** $t = 2$ to T **do**
 - 8: $\theta^{(t)} \leftarrow \lambda_{\text{shrink}} \theta^{(t-1)} + \lambda_{\text{perturb}} \epsilon^{(t)}$
 - 9: **for** $i = 1$ to epoch_{ws} **do**
 - 10: Predict $x^{(t)}$ via $\mathcal{A}(G_p^{(t)}; \theta^{(t)})$
 - 11: Update $\theta^{(t)}$ using $\nabla \ell(x^{(t)}; Q_p^{(t)})$
 - 12: **end for**
 - 13: **end for**
-

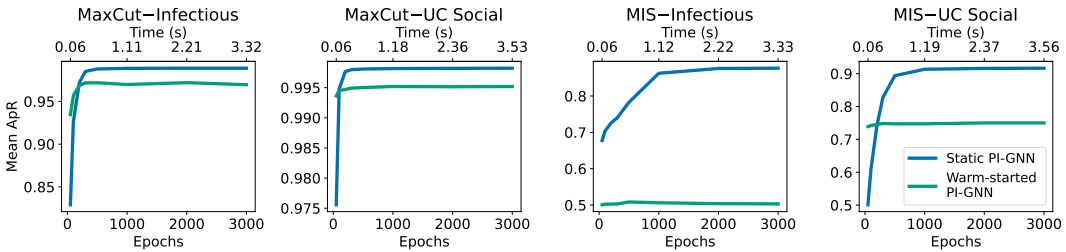


Figure 1: Performance of static PI-GNN and warm-started PI-GNN on dynamic MaxCut and MIS instances. Detailed setup is explained in Section 5.

These phenomena are closely tied to the role of initialization in deep learning [11, 16, 45] and can be attributed to the highly nonconvex nature of the optimization objective with respect to the model parameters, which gives rise to numerous local optima. When the first snapshot is optimized to convergence, the model undergoes extensive optimization, resulting in increased confidence in its predictions. Consequently, when the model is warm-started, the gradients become small due to this overconfidence, making it more difficult for the model to escape local optima. This hampers its ability to discover higher-quality solutions despite faster initial progress.

4.2 DyCO-GNN: fast convergence and robust solution quality

To address the shortcomings of naively warm-starting PI-GNN, we propose DyCO-GNN—a simple yet effective method that facilitates both fast convergence and robust solution quality across graph snapshots. Unlike standard warm start, which reuses the exact model parameters from the previous snapshot, DyCO-GNN integrates a strategic initialization method—shrink and perturb (SP) [2]. The goal is to retain the benefits of accelerated convergence while mitigating the tendency of the model to become trapped in suboptimal local minima due to overconfident predictions caused by warm start.

SP was originally designed to close the generalization gap caused by naively warm-starting neural network training. It shrinks the model parameters and then adds perturbation noise. Shrinking the parameters effectively decreases the model’s confidence while preserving the learned hypothesis. Adding noise empirically improves training time and test performance. It is important to note that there is no notion of generalization in our method as the model parameters are independently optimized for each individual problem instance snapshot. Despite the fact that SP tackles a different problem, we successfully adopt it to resolve the issues of warm-started PI-GNN.

When a new snapshot $G_p^{(t)}$ arrives, DyCO-GNN applies SP to the warm-started parameters before starting the optimization process. The newly initialized parameters are defined as

$$\theta^{(t)} \leftarrow \lambda_{\text{shrink}} \theta^{(t-1)} + \lambda_{\text{perturb}} \epsilon^{(t)},$$

where $0 < \lambda_{\text{shrink}} < 1$, $0 < \lambda_{\text{perturb}} < 1$, and $\epsilon^{(t)} \sim \mathcal{N}(0, \sigma^2)$. With the reintroduced gradient diversity and disrupted premature overconfidence, DyCO-GNN effectively escapes the local minima in the loss landscape. This gentle destabilization promotes exploration of alternative descent paths, functioning as a principled soft reset mechanism that facilitates more effective and robust optimization.

With this simple design, DyCO-GNN achieves a balanced trade-off: it preserves the efficiency of warm start under tight time constraints while enabling the model to reach higher-quality solutions as more computational budget becomes available. The pseudocode of DyCO-GNN is provided in Algorithm 2. As we show in Section 5, DyCO-GNN consistently outperforms warm-started PI-GNN across DCO problems such as dynamic MaxCut, MIS, and TSP, particularly under moderate to generous time budgets where naive warm start fails to find high-quality solutions effectively. We will also show that DyCO-GNN finds better solutions than the converged static PI-GNN much faster.

4.3 Theoretical support

We analytically support the advantage of SP over warm start. The theorem is based on the Goemans and Williamson [13] (GW) algorithm, the best-known optimization algorithm for solving MaxCut. The GW algorithm is structured similar to DyCO-GNN, but with a more computationally intensive QUBO relaxation (an SDP) and rounding step (randomized projections). We adopt it to show that the advantage of SP persists even if we advance the relaxation and rounding steps.

Theorem 1. *Fix the solution X_0 of the GW SDP step, and define $X_\lambda := \text{Proj}_{\mathcal{X}}(X_0 + \lambda Z)$, where $\lambda \in \mathbb{R}_{>0}$, Z is a symmetric random matrix sampled from the Gaussian Orthogonal Ensemble, and $\text{Proj}_{\mathcal{X}}(\cdot)$ is projection onto set $\mathcal{X} = \{X \mid X \succeq 0, \text{diag}(X) = 1\}$. Denote the GW rounding step by $R : \{\mathcal{X}, \Omega\} \rightarrow \{0, 1, \dots, c^*\}$, where Ω is the random seed set of the cut plane and c^* is the maximum achievable cut size. Let $C_{\text{opt}} = \{X \in \mathcal{X} : \mathbb{P}_\Omega(R(X, \omega) = c^*) > 0\}$. Assume that the set C_{opt} has positive Lebesgue measure in \mathcal{X} , and that $X_0 \notin C_{\text{opt}}$. Then, there exists a $\lambda > 0$ such that*

$$\mathbb{P}_{\Omega, Z}(R(X_\lambda, \omega) = c^*) > \mathbb{P}_\Omega(R(X_0, \omega) = c^*) = 0.$$

In words, the theorem shows that (pre-rounding) perturbations can strictly increase the probability of finding the optimal cut. The proof is shown in Appendix D, along with a detailed description of the GW algorithm, and a corollary extending the result to perturbations of the GW SDP initialization.

5 Experiments

We empirically evaluate DyCO-GNN on dynamic instances of MaxCut, MIS, and TSP of varying problem sizes. Baselines include static PI-GNN and warm-started PI-GNN. We exclude methods that rely on extensive offline training across instance distributions. This choice aligns with the core design philosophy of our proposed approach, which, like PI-GNN, emphasizes *instance-specific adaptability* over generalization. While generalizable methods trained on large datasets may offer strong performance on similar distributions, prior research has shown that methods from the PI-GNN family often achieve comparable performance across static CO problems like MaxCut and MIS [19, 42, 51]. Moreover, the generalization gap of the methods with generalizability increases significantly when distribution shift is present [25, 51]. By focusing our comparison on methods within the PI-GNN family, we provide a clearer assessment of the algorithmic innovations without conflating results with the (dis)advantages of dataset-level generalization.

5.1 Datasets

We utilized established graph datasets that contain temporal information to ensure that the dynamic evolution of the graphs accurately reflects realistic, time-dependent structural changes. This approach allows us to capture authentic patterns of change within the graph over time, thereby enhancing the validity and applicability of our experimental results. We summarize the statistics of the original and preprocessed datasets in Table 1.

Table 1: Statistics of all datasets. Original edges can be directed and have duplicates.

Dataset	Original		Preprocessed		Δ edges
	Nodes	Edges	Nodes	Edges	
Infectious	410	17,298	410	2765	~ 276 (10%)
UC Social	1899	59,835	1899	13,838	~ 1384 (10%)
DBLP	12,590	49,759	12,590	49,636	~ 993 (2%)
burma14	14	91	15	105	-
ulysses22	22	213	23	253	-
st70	70	2,415	71	2,485	-

For MaxCut and MIS, we employed Infectious [21], a human contact network; UC Social [36], a communication network; and DBLP [31], a citation network. All datasets are publicly available in the Koblenz Network Collection [30]. Each dataset is a graph with timestamps attached to all edges. For preprocessing, we began by sorting all edge events in chronological order, followed by the removal of self-loops and duplicate edges. Finally, we made all graphs undirected. To construct DTDG snapshots for MaxCut, we converted the graphs into 10 snapshots by linearly increasing the number of edges to include in each of them (i.e., the dynamic graph grows over time). For Infectious and UC Social, we added $\sim 10\%$ of total edges of the final graph every step; for DBLP, we added $\sim 2\%$ each step, considering its total number of edges is much larger. Edge additions will lead to MIS constraint violations. In that case, a postprocessing step that reuses previous solutions and removes violations would be sufficient to solve the DCO problem. Therefore, to construct DTDG snapshots for MIS, we reversed the snapshot order and turn edge additions into edge deletions.

For TSP, we first took static TSP benchmark problems from TSPLIB [40]. Specifically, we considered burma14, ulysses22, and st70. We added an extra node and let it move along a straight line within the region defined by the other existing nodes. We recorded the coordinates of 5 equally spaced locations along the trajectory (i.e., 5 snapshots in total).

5.2 Implementation details

DyCO-GNN consists of a node embedding layer and two graph convolution layers. Unlike previous works [17, 19, 42] that used different embedding and intermediate hidden dimensions for each problem instance, we used 512 for the embedding dimension and 256 for the hidden dimension in all our experiments. We experimented with the graph convolution operator (GCNConv) from [28] and the GraphSAGE operator (SAGEConv) from [15]. We found that DyCO-GNN with GCNConv failed to find good enough solutions to TSP, so we only report results of the SAGEConv models on dynamic TSP. We set $\lambda_{\text{shrink}} = 0.4$ and $\lambda_{\text{perturb}} = 0.1$ without further tuning. All MaxCut and MIS experiments were repeated five times; all TSP experiments were repeated ten times. We obtained the ground truth for each snapshot by formulating it as a QUBO problem and solving it using the Gurobi solver [14] with a time limit of 60 seconds. Additional implementation details are provided in Appendix B.

5.3 Empirical results on DCO problems

Tables 2, 3, and 4 report the mean ApR of all methods on dynamic MaxCut, MIS, and TSP, respectively. We also evaluate variants of DyCO-GNN that apply SP to different layers of DyCO-GNN. For MaxCut and MIS, results are reported using the final model checkpoint. For TSP, both the final and the best-performing checkpoints are considered. The wall-clock time of the best-performing checkpoint includes the total decoding time over all checkpoints available. As noted in Section 4, the advantage of warm-started PI-GNN compared to static PI-GNN diminishes quickly when we relax the runtime constraint. DyCO-GNN closes this performance gap and consistently outperforms static PI-GNN and warm-started PI-GNN across all problems and datasets. Even on a strict budget (first column of each table), DyCO-GNN surpasses warm-started PI-GNN in most cases. Crucially, DyCO-GNN consistently finds better solutions than fully converged static PI-GNN, and often within just **1.67%** to **33.33%** of the total runtime. This improvement possibly stems from information carryover and continual learning on a similar graph structure, enabled by the utilization of the previously learned hypothesis. Although the three versions of DyCO-GNN give strong results, no single setting dominates all tasks and datasets. We will discuss the implications in Section 6. We visualize snapshot-level ApRs under different time budgets in Figures 2, 3, and 4. Notably, DyCO-GNN maintains its edge across almost all evaluated snapshots, confirming its robustness. Additional experimental results are provided in Appendix C.

Table 2: Mean ApR on dynamic MaxCut. Values closer to 1 are better (\uparrow). All methods use GCNConv. “emb”, “GNN”, and “full” refer to applying SP to the embedding layer, GNN layers, and all layers, respectively. The best result for each time budget is in bold. The first time each method surpasses the converged solution of static PI-GNN is highlighted.

Time budget (epochs/seconds)									
	Method	50/0.06	100/0.12	200/0.23	300/0.34	500/0.56	1000/1.11	2000/2.21	3000/3.32
Infectious	PI-GNN (static)	0.82906	0.92646	0.97203	0.98509	0.98801	0.98871	0.98887	0.98888
	PI-GNN (warm)	0.93460	0.95681	0.96874	0.97170	0.97186	0.96980	0.97196	0.96959
	DyCO-GNN (emb)	0.88562	0.96018	0.97817	0.98458	0.97695	0.97874	0.98117	0.96473
	DyCO-GNN (GNN)	0.93187	0.96485	0.97962	0.98366	0.98478	0.98456	0.98460	0.98409
	DyCO-GNN (full)	0.86286	0.96830	0.98384	0.98793	0.98947	0.98878	0.98869	0.98836
Time budget (epochs/seconds)									
	Method	50/0.06	100/0.12	200/0.24	300/0.36	500/0.59	1000/1.18	2000/2.36	3000/3.53
UC Social	PI-GNN (static)	0.97557	0.99485	0.99764	0.99798	0.99809	0.99817	0.99820	0.99823
	PI-GNN (warm)	0.99363	0.99455	0.99469	0.99492	0.99501	0.99519	0.99515	0.99519
	DyCO-GNN (emb)	0.99634	0.99709	0.99734	0.99720	0.99711	0.99710	0.99711	0.99705
	DyCO-GNN (GNN)	0.99352	0.99714	0.99779	0.99781	0.99786	0.99782	0.99782	0.99779
	DyCO-GNN (full)	0.99404	0.99724	0.99825	0.99841	0.99843	0.99848	0.99846	0.99848
Time budget (epochs/seconds)									
	Method	50/0.14	100/0.29	200/0.57	300/0.85	500/1.41	1000/2.82	2000/5.63	3000/8.44
DBLP	PI-GNN (static)	0.80083	0.97292	0.98905	0.98973	0.99017	0.99054	0.99081	0.99095
	PI-GNN (warm)	0.98804	0.98890	0.98957	0.98969	0.98976	0.99001	0.99009	0.99039
	DyCO-GNN (emb)	0.98858	0.98995	0.99028	0.99039	0.99044	0.99047	0.99061	0.99041
	DyCO-GNN (GNN)	0.98950	0.99110	0.99145	0.99155	0.99164	0.99176	0.99180	0.99183
	DyCO-GNN (full)	0.99319	0.99515	0.99524	0.99515	0.99509	0.99495	0.99484	0.99477

Table 3: Mean ApR on dynamic MIS. Values closer to 1 are better (\uparrow). All methods use GCNConv. “emb”, “GNN”, and “full” refer to applying SP to the embedding layer, GNN layers, and all layers, respectively. The best result for each time budget is in bold. The first time each method surpasses the converged solution of static PI-GNN is highlighted.

Time budget (epochs/seconds)									
	Method	50/0.06	100/0.12	200/0.23	300/0.34	500/0.56	1000/1.12	2000/2.22	3000/3.33
Infectious	PI-GNN (static)	0.67757	0.70395	0.72587	0.73944	0.78275	0.86258	0.87577	0.87651
	PI-GNN (warm)	0.50072	0.50217	0.50255	0.50285	0.50845	0.50620	0.50381	0.50309
	DyCO-GNN (emb)	0.78941	0.79577	0.77912	0.76798	0.74713	0.72983	0.72221	0.70964
	DyCO-GNN (GNN)	0.69457	0.74386	0.79747	0.78105	0.75516	0.73314	0.71517	0.71508
	DyCO-GNN (full)	0.69461	0.72760	0.75278	0.77278	0.84044	0.88254	0.88397	0.88515
Time budget (epochs/seconds)									
	Method	50/0.06	100/0.12	200/0.24	300/0.36	500/0.60	1000/1.19	2000/2.37	3000/3.56
UC Social	PI-GNN (static)	0.50103	0.60923	0.74196	0.82713	0.89385	0.91340	0.91594	0.91655
	PI-GNN (warm)	0.73879	0.74222	0.74561	0.74828	0.74731	0.74740	0.75011	0.75016
	DyCO-GNN (emb)	0.87396	0.86808	0.85321	0.84667	0.83863	0.82997	0.82259	0.81732
	DyCO-GNN (GNN)	0.68646	0.78990	0.82860	0.82898	0.82632	0.82217	0.81881	0.81739
	DyCO-GNN (full)	0.54819	0.66512	0.80108	0.87445	0.91600	0.92037	0.92069	0.91984
Time budget (epochs/seconds)									
	Method	50/0.14	100/0.28	200/0.57	300/0.85	500/1.40	1000/2.80	2000/5.60	3000/8.41
DBLP	PI-GNN (static)	0.18364	0.48119	0.89690	0.93320	0.94304	0.94636	0.94766	0.94813
	PI-GNN (warm)	0.93136	0.93313	0.93459	0.93516	0.93595	0.93672	0.93771	0.93925
	DyCO-GNN (emb)	0.95517	0.95599	0.95529	0.95491	0.95478	0.95398	0.95446	0.95448
	DyCO-GNN (GNN)	0.73970	0.93442	0.94082	0.94114	0.94119	0.94135	0.94169	0.94183
	DyCO-GNN (full)	0.26570	0.65637	0.95175	0.96550	0.96895	0.96972	0.97016	0.97042

Sensitivity of different methods to varying degrees of change. Tables 2 and 3 show that the quality gap of converged solutions between static PI-GNN and DyCO-GNN (resp. warm-started PI-GNN) is larger (resp. smaller) for DBLP. This is because we constructed the DTDG for DBLP with a smaller relative change in the edge set (~2% of total edges), which leads to greater structural overlaps. Consequently, warm-started PI-GNN and DyCO-GNN would be stronger in such a scenario. We further conducted a sensitivity analysis by varying the degrees of change in the DTDGs. Results are illustrated in Figure 5. When Δ_{edges} is getting smaller, the gap between static and warm-started PI-GNN is narrowed, and the advantage of DyCO-GNN compared to static PI-GNN is more salient, which is consistent with our hypothesis.

Table 4: Mean ApR on dynamic TSP. Values closer to 1 are better (\downarrow). The best-performing checkpoint was taken. ‘‘emb’’, ‘‘GNN’’, and ‘‘full’’ refer to applying SP to the embedding layer, GNN layers, and all layers, respectively. The best result for each time budget is in bold. The first time each method surpasses the converged solution of static PI-GNN is highlighted.

		Time budget (epochs/seconds)							
		Method	500/0.31	1000/0.62	2000/1.24	3000/1.86	5000/3.10	10000/6.21	-
burma14	PI-GNN (static)	1.31234	1.13584	1.06970	1.05998	1.04756	1.03358	-	
	PI-GNN (warm)	1.28388	1.28313	1.25798	1.23433	1.21120	1.13860	-	
	DyCO-GNN (emb)	1.15106	1.13302	1.09256	1.07814	1.06478	1.04782	-	
	DyCO-GNN (GNN)	1.10365	1.06370	1.05406	1.05668	1.03737	1.01811	-	
	DyCO-GNN (full)	1.15884	1.10839	1.04531	1.03134	1.03160	1.04032	-	
		Time budget (epochs/seconds)							
		Method	500/0.32	1000/0.64	2000/1.27	3000/1.90	5000/3.18	10000/6.37	-
ulysses22	PI-GNN (static)	1.76783	1.48249	1.26151	1.17969	1.11249	1.08867	-	
	PI-GNN (warm)	1.18266	1.17228	1.18642	1.18381	1.17534	1.19563	-	
	DyCO-GNN (emb)	1.20391	1.16486	1.16819	1.15758	1.14706	1.13088	-	
	DyCO-GNN (GNN)	1.25758	1.19970	1.14971	1.12991	1.12469	1.13545	-	
	DyCO-GNN (full)	1.30026	1.27399	1.22204	1.16843	1.12538	1.08516	-	
		Time budget (epochs/seconds)							
		Method	500/0.43	1000/0.85	2000/1.70	3000/2.54	5000/4.23	10000/8.46	20000/16.95
st70	PI-GNN (static)	2.01621	1.98448	1.92607	1.82142	1.59433	1.43824	1.36945	
	PI-GNN (warm)	1.47258	1.46055	1.42443	1.42589	1.38696	1.36187	1.34213	
	DyCO-GNN (emb)	1.45563	1.42486	1.38436	1.36485	1.35266	1.30753	1.29239	
	DyCO-GNN (GNN)	1.53036	1.44924	1.36227	1.33620	1.32063	1.27857	1.23655	
	DyCO-GNN (full)	1.56795	1.54532	1.38231	1.34845	1.30566	1.27127	1.24412	

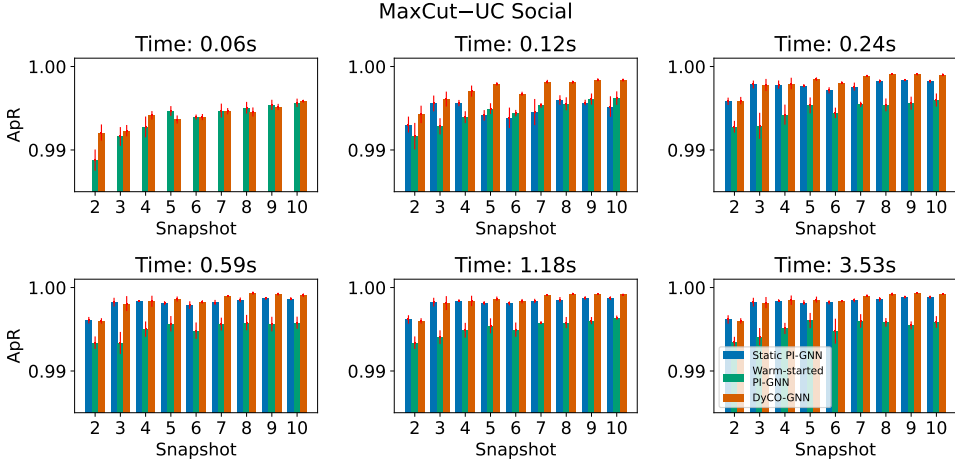


Figure 2: Snapshot-level ApRs on dynamic MaxCut instance (UC Social). All methods use GCNConv.

6 Discussion

Limitations and future work. In our experiments, most hyperparameters were either kept at their default settings or chosen with minimal tuning. The performance of DyCO-GNN can likely be further improved by tuning the model architecture and optimizer using the snapshot(s) available at hand, and incorporating techniques such as learning rate scheduling. We have shown that applying SP to different layers of DyCO-GNN yields varying performance. A promising direction for future work is to make the SP step adaptive. Currently, the embedding layer and the GNN layers are jointly optimized without explicit decoupling. By introducing appropriate regularization strategies or auxiliary loss functions, we can promote distinct functional roles across layers—for instance, encouraging the embedding layer to capture representations specific to both the problem and graph structure and the GNN layers to learn to aggregate such representations. Additionally, if we evaluate the likelihood of changes in node assignments under dynamic conditions based on certain heuristics, it becomes possible to apply SP in a node-wise, adaptive manner. Another promising extension is to combine DyCO-GNN with the continuous relaxation annealing (CRA) technique proposed in [19] to enhance the solution quality, particularly on dense graphs.

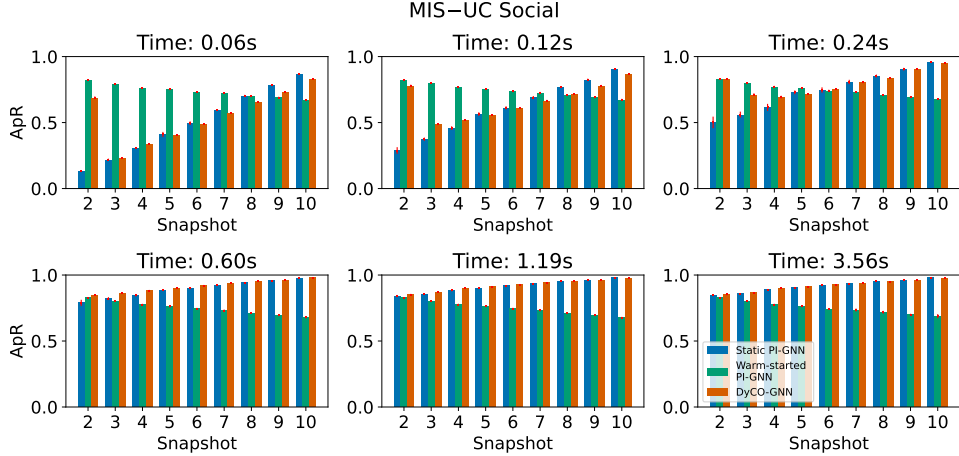


Figure 3: Snapshot-level ApRs on dynamic MIS instance (UC Social). All methods use GCNConv.

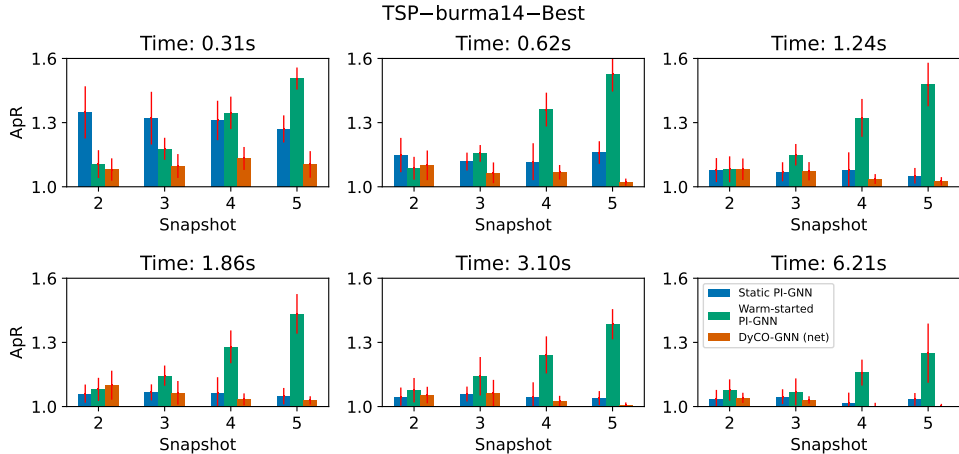


Figure 4: Snapshot-level ApRs on dynamic TSP instance (burma14). The best checkpoint was taken.

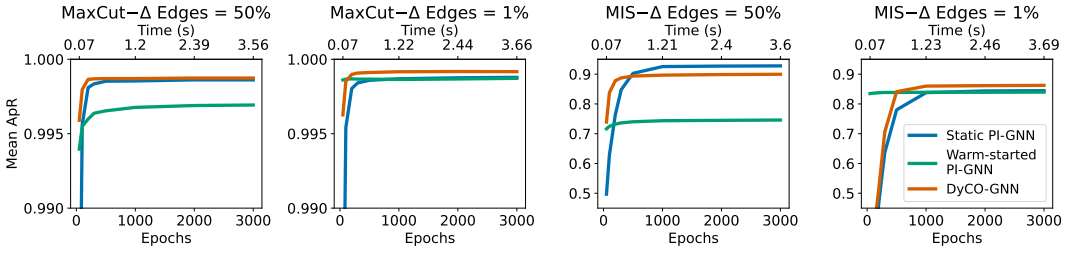


Figure 5: Sensitivity analysis using UC Social.

Conclusion. We introduced DyCO-GNN, the first learning-based framework designed to solve DCO problems. Through extensive experiments on dynamic MaxCut, MIS, and TSP, we demonstrated that DyCO-GNN consistently outperforms both static and warm-started PI-GNN baselines under varying runtime constraints and across diverse problem settings. Our analysis reveals that DyCO-GNN achieves superior solution quality even under strict time budgets, always surpassing the best-performing checkpoints of the baseline methods in a fraction of their runtime. These improvements are significant in rapidly changing environments, where timely decision-making is critical. Furthermore, DyCO-GNN’s ability to efficiently adapt to evolving problem instance snapshots without optimization from scratch or external supervision underscores its potential for real-world deployment in dynamic, resource-constrained settings.

References

- [1] Rico Angell and Andrew Mccallum. Fast, scalable, warm-start semidefinite programming with spectral bundling and sketching. In *International Conference on Machine Learning*, pages 1579–1615. PMLR, 2024.
- [2] Jordan Ash and Ryan P Adams. On warm-starting neural network training. *Advances in neural information processing systems*, 33:3884–3894, 2020.
- [3] Sepehr Assadi, Krzysztof Onak, Baruch Schieber, and Shay Solomon. Fully dynamic maximal independent set with sublinear update time. In *Proceedings of the 50th Annual ACM SIGACT Symposium on theory of computing*, pages 815–826, 2018.
- [4] Giorgio Ausiello, Bruno Escoffier, Jérôme Monnot, and Vangelis Paschos. Reoptimization of minimum and maximum traveling salesman’s tours. *Journal of Discrete Algorithms*, 7(4):453–463, 2009.
- [5] Heinz H Bauschke and Patrick L Combettes. *Convex analysis and monotone operator theory in Hilbert spaces*. Springer, 2017.
- [6] Irwan Bello, Hieu Pham, Quoc V Le, Mohammad Norouzi, and Samy Bengio. Neural combinatorial optimization with reinforcement learning. *arXiv preprint arXiv:1611.09940*, 2016.
- [7] Michaël Defferrard, Xavier Bresson, and Pierre Vandergheynst. Convolutional neural networks on graphs with fast localized spectral filtering. *Advances in neural information processing systems*, 29, 2016.
- [8] Hristo N Djidjev, Guillaume Chapuis, Georg Hahn, and Guillaume Rizk. Efficient combinatorial optimization using quantum annealing. *arXiv preprint arXiv:1801.08653*, 2018.
- [9] Matthias Fey and Jan Eric Lenssen. Fast graph representation learning with pytorch geometric. *arXiv preprint arXiv:1903.02428*, 2019.
- [10] Maxime Gasse, Didier Chételat, Nicola Ferroni, Laurent Charlin, and Andrea Lodi. Exact combinatorial optimization with graph convolutional neural networks. *Advances in neural information processing systems*, 32, 2019.
- [11] Xavier Glorot and Yoshua Bengio. Understanding the difficulty of training deep feedforward neural networks. In *Proceedings of the thirteenth international conference on artificial intelligence and statistics*, pages 249–256. JMLR Workshop and Conference Proceedings, 2010.
- [12] Fred Glover, Gary Kochenberger, and Yu Du. A tutorial on formulating and using qubo models. *arXiv preprint arXiv:1811.11538*, 2018.
- [13] Michel X Goemans and David P Williamson. Improved approximation algorithms for maximum cut and satisfiability problems using semidefinite programming. *Journal of the ACM (JACM)*, 42(6):1115–1145, 1995.
- [14] Gurobi Optimization, LLC. Gurobi Optimizer Reference Manual, 2024. URL <https://www.gurobi.com>.
- [15] Will Hamilton, Zhitao Ying, and Jure Leskovec. Inductive representation learning on large graphs. *Advances in neural information processing systems*, 30, 2017.
- [16] Kaiming He, Xiangyu Zhang, Shaoqing Ren, and Jian Sun. Delving deep into rectifiers: Surpassing human-level performance on imagenet classification. In *Proceedings of the IEEE international conference on computer vision*, pages 1026–1034, 2015.
- [17] Nasimeh Heydaribeni, Xinrui Zhan, Ruisi Zhang, Tina Eliassi-Rad, and Farinaz Koushanfar. Distributed constrained combinatorial optimization leveraging hypergraph neural networks. *Nature Machine Intelligence*, pages 1–9, 2024.
- [18] Benjamin Hudson, Qingbiao Li, Matthew Malencia, and Amanda Prorok. Graph neural network guided local search for the traveling salesperson problem. In *International Conference on Learning Representations*, 2022.

- [19] Yuma Ichikawa. Controlling continuous relaxation for combinatorial optimization. In *The Thirty-eighth Annual Conference on Neural Information Processing Systems*, 2024.
- [20] The MathWorks Inc. Traveling salesperson problem with qubo, 2024. URL <https://www.mathworks.com/help/matlab/math/quantum-tsp.html>.
- [21] Lorenzo Isella, Juliette Stehlé, Alain Barrat, Ciro Cattuto, Jean-François Pinton, and Wouter Van den Broeck. What's in a crowd? analysis of face-to-face behavioral networks. *Journal of theoretical biology*, 271(1):166–180, 2011.
- [22] Elizabeth John and E Alper Yıldırım. Implementation of warm-start strategies in interior-point methods for linear programming in fixed dimension. *Computational Optimization and Applications*, 41(2):151–183, 2008.
- [23] Chaitanya K Joshi, Thomas Laurent, and Xavier Bresson. An efficient graph convolutional network technique for the travelling salesman problem. *arXiv preprint arXiv:1906.01227*, 2019.
- [24] Chaitanya K Joshi, Quentin Cappart, Louis-Martin Rousseau, and Thomas Laurent. Learning the travelling salesperson problem requires rethinking generalization. *Constraints*, 27(1):70–98, 2022.
- [25] Nikolaos Karalias and Andreas Loukas. Erdos goes neural: an unsupervised learning framework for combinatorial optimization on graphs. *Advances in Neural Information Processing Systems*, 33:6659–6672, 2020.
- [26] Elias Khalil, Hanjun Dai, Yuyu Zhang, Bistra Dilkina, and Le Song. Learning combinatorial optimization algorithms over graphs. *Advances in neural information processing systems*, 30, 2017.
- [27] Diederik P. Kingma and Jimmy Ba. Adam: A method for stochastic optimization. In *International Conference on Learning Representations*, 2015.
- [28] Thomas N. Kipf and Max Welling. Semi-supervised classification with graph convolutional networks. In *International Conference on Learning Representations*, 2017.
- [29] Wouter Kool, Herke van Hoof, and Max Welling. Attention, learn to solve routing problems! In *International Conference on Learning Representations*, 2019.
- [30] Jérôme Kunegis. Konect: the koblenz network collection. In *Proceedings of the 22nd international conference on world wide web*, pages 1343–1350, 2013.
- [31] Michael Ley. The dblp computer science bibliography: Evolution, research issues, perspectives. In *International symposium on string processing and information retrieval*, pages 1–10. Springer, 2002.
- [32] Yang Li, Jinpei Guo, Runzhong Wang, and Junchi Yan. T2t: From distribution learning in training to gradient search in testing for combinatorial optimization. *Advances in Neural Information Processing Systems*, 36:50020–50040, 2023.
- [33] Yang Li, Jinpei Guo, Runzhong Wang, Hongyuan Zha, and Junchi Yan. Fast t2t: Optimization consistency speeds up diffusion-based training-to-testing solving for combinatorial optimization. *Advances in Neural Information Processing Systems*, 37:30179–30206, 2024.
- [34] Andrew Lucas. Ising formulations of many np problems. *Frontiers in physics*, 2:5, 2014.
- [35] Krzysztof Onak and Ronitt Rubinfeld. Maintaining a large matching and a small vertex cover. In *Proceedings of the forty-second ACM symposium on Theory of computing*, pages 457–464, 2010.
- [36] Tore Opsahl and Pietro Panzarasa. Clustering in weighted networks. *Social networks*, 31(2):155–163, 2009.
- [37] Christos H. Papadimitriou and Kenneth Steiglitz. *Combinatorial optimization: algorithms and complexity*. Prentice-Hall, Inc., USA, 1982. ISBN 0131524623.

- [38] Adam Paszke, Sam Gross, Francisco Massa, Adam Lerer, James Bradbury, Gregory Chanan, Trevor Killeen, Zeming Lin, Natalia Gimelshein, Luca Antiga, Alban Desmaison, Andreas Köpf, Edward Yang, Zach DeVito, Martin Raison, Alykhan Tejani, Sasank Chilamkurthy, Benoit Steiner, Lu Fang, Junjie Bai, and Soumith Chintala. Pytorch: an imperative style, high-performance deep learning library. In *Proceedings of the 33rd International Conference on Neural Information Processing Systems*, 2019.
- [39] Ruizhong Qiu, Zhiqing Sun, and Yiming Yang. Dimes: A differentiable meta solver for combinatorial optimization problems. *Advances in Neural Information Processing Systems*, 35: 25531–25546, 2022.
- [40] Gerhard Reinelt. Tsplib - a traveling salesman problem library. *INFORMS J. Comput.*, 3: 376–384, 1991. URL <https://api.semanticscholar.org/CorpusID:207225504>.
- [41] Sebastian Sanokowski, Wilhelm Berghammer, Sepp Hochreiter, and Sebastian Lehner. Variational annealing on graphs for combinatorial optimization. *Advances in Neural Information Processing Systems*, 36:63907–63930, 2023.
- [42] Martin JA Schuetz, J Kyle Brubaker, and Helmut G Katzgraber. Combinatorial optimization with physics-inspired graph neural networks. *Nature Machine Intelligence*, 4(4):367–377, 2022.
- [43] Alexander Shapiro. Sensitivity analysis of nonlinear programs and differentiability properties of metric projections. *SIAM Journal on Control and Optimization*, 26(3):628–645, 1988.
- [44] Zhiqing Sun and Yiming Yang. Difusco: Graph-based diffusion solvers for combinatorial optimization. *Advances in neural information processing systems*, 36:3706–3731, 2023.
- [45] Ilya Sutskever, James Martens, George Dahl, and Geoffrey Hinton. On the importance of initialization and momentum in deep learning. In *International conference on machine learning*, pages 1139–1147. PMLR, 2013.
- [46] Mikkel Thorup. Fully-dynamic min-cut. *Combinatorica*, 27(1):91–127, 2007.
- [47] Jan Toenshoff, Martin Ritzert, Hinrikus Wolf, and Martin Grohe. Graph neural networks for maximum constraint satisfaction. *Frontiers in artificial intelligence*, 3:580607, 2021.
- [48] Jan Tönshoff, Berke Kisín, Jakob Lindner, and Martin Grohe. One model, any csp: graph neural networks as fast global search heuristics for constraint satisfaction. In *Proceedings of the Thirty-Second International Joint Conference on Artificial Intelligence, IJCAI ’23*, 2023.
- [49] Petar Veličković, Guillem Cucurull, Arantxa Casanova, Adriana Romero, Pietro Liò, and Yoshua Bengio. Graph attention networks. In *International Conference on Learning Representations*, 2018.
- [50] Oriol Vinyals, Meire Fortunato, and Navdeep Jaitly. Pointer networks. *Advances in neural information processing systems*, 28, 2015.
- [51] Haoyu Peter Wang and Pan Li. Unsupervised learning for combinatorial optimization needs meta learning. In *The Eleventh International Conference on Learning Representations*, 2023.
- [52] Omer Wasim and Valerie King. Fully dynamic sequential and distributed algorithms for max-cut. In *40th IARCS Annual Conference on Foundations of Software Technology and Theoretical Computer Science (FSTTCS 2020)*, pages 33–1. Schloss Dagstuhl–Leibniz-Zentrum für Informatik, 2020.
- [53] Shengxiang Yang, Yong Jiang, and Trung Thanh Nguyen. Metaheuristics for dynamic combinatorial optimization problems. *IMA Journal of Management Mathematics*, 24(4):451–480, 10 2012. ISSN 1471-6798. doi: 10.1093/imaman/dps021.
- [54] E Alper Yildirim and Stephen J Wright. Warm-start strategies in interior-point methods for linear programming. *SIAM Journal on Optimization*, 12(3):782–810, 2002.
- [55] Zizhen Zhang, Hong Liu, MengChu Zhou, and Jiahai Wang. Solving dynamic traveling salesman problems with deep reinforcement learning. *IEEE Transactions on Neural Networks and Learning Systems*, 34(4):2119–2132, 2021.

A Additional related work

DCO problems have been addressed from a theoretical perspective [35, 46], including for the dynamic MaxCut [52], MIS [3], and TSP [4] problems, as well as from the perspective of designing heuristics [53]. Our work brings a learning-based approach to this line of work.

The idea of warm-starting semidefinite programs in general, and the starting solutions of interior-point methods (which can be used to solved SDPs, among other problem classes) has been explored from a theoretical perspective [1, 22, 54]. Our theoretical findings complement this literature by exploring the impacts of warm-starting SDP solutions for the MaxCut problem. Our learning-based method DyCO-GNN also brings similar ideas into the realm of learning-based DCO methods.

B Additional implementation details

We used the Adam optimizer [27]; the learning rate was set to 0.001 for all MaxCut and MIS experiments, 0.0002 for burma14 and st70, and 0.0005 for ulysses22. As described in Algorithms 1 and 2, we optimize over the first snapshot for epoch_{\max} epochs. Thus, we skip the first snapshot during evaluation since the results will be identical across all methods. We set $\text{epoch}_{\max} = 3000$ for all MaxCut and MIS experiments, $\text{epoch}_{\max} = 10000$ for burma14 and ulysses22, and $\text{epoch}_{\max} = 20000$ for st70.

The penalty term M was set to 2 for MIS and $2 \times \max_{(i,j) \in E} w_{ij}$ (i.e., $2 \times$ the max distance between any two nodes) for TSP. For MIS, we postprocessed the output of our model by greedily removing violations. For TSP, we decoded the route step by step. More specifically, for burma14 and ulysses22, we discarded nodes that have already been visited and selected the most likely node to visit based on our model output; for st70, we found that this greedy decoding failed to find good enough routes and instead applied beam search that expands the top 5 possible valid nodes at each step.

All models were implemented using PyTorch [38] and PyTorch Geometric [9]. Experiments were conducted on a machine with a single NVIDIA GeForce RTX 4090 GPU, a 32-core Intel Core i9-14900K CPU, and 64 GB of RAM running Ubuntu 24.04.

C Additional experimental results

C.1 DyCO-GNN with SAGEConv for dynamic Maxcut and MIS

Table 5: Mean ApR on dynamic MaxCut. Values closer to 1 are better (\uparrow). All methods use SAGEConv. The best result for each time budget is in bold. The first time each method surpasses the converged solution of static PI-GNN is highlighted.

		Time budget (epochs/seconds)							
		50/0.06	100/0.12	200/0.23	300/0.34	500/0.56	1000/1.11	2000/2.21	3000/3.32
Infectious	PI-GNN (static)	0.97028	0.97353	0.97487	0.97540	0.97570	0.97591	0.97626	0.97636
	PI-GNN (warm)	0.95685	0.96117	0.96356	0.96452	0.96396	0.96625	0.96841	0.96619
	DyCO-GNN (full)	0.97771	0.97854	0.97880	0.97953	0.97952	0.97959	0.98051	0.98009
		Time budget (epochs/seconds)							
		50/0.06	100/0.12	200/0.24	300/0.36	500/0.59	1000/1.18	2000/2.36	3000/3.53
UC Social	PI-GNN (static)	0.98875	0.99601	0.99714	0.99727	0.99766	0.99768	0.99773	0.99782
	PI-GNN (warm)	0.99292	0.99395	0.99440	0.99456	0.99451	0.99447	0.99437	0.99456
	DyCO-GNN (full)	0.99515	0.99584	0.99595	0.99594	0.99593	0.99589	0.99856	0.99852
		Time budget (epochs/seconds)							
		50/0.14	100/0.29	200/0.57	300/0.85	500/1.41	1000/2.82	2000/5.63	3000/8.44
DBLP	PI-GNN (static)	0.89694	0.92001	0.93263	0.93688	0.94120	0.94487	0.94610	0.94659
	PI-GNN (warm)	0.94865	0.95037	0.95249	0.95282	0.95336	0.95477	0.95337	0.95444
	DyCO-GNN (full)	0.95877	0.95942	0.95981	0.95971	0.95965	0.95944	0.95934	0.95907

Table 6: Mean ApR on dynamic MIS. Values closer to 1 are better (\uparrow). All methods use SAGEConv. The best result for each time budget is in bold. The first time each method surpasses the converged solution of static PI-GNN is highlighted.

Time budget (epochs/seconds)								
Method	50/0.06	100/0.12	200/0.23	300/0.34	500/0.56	1000/1.12	2000/2.22	3000/3.33
Infectious	PI-GNN (static)	0.79468	0.91679	0.95948	0.96362	0.96410	0.96476	0.96518
	PI-GNN (warm)	0.96725	0.96713	0.96727	0.96708	0.96701	0.96717	0.96715
	DyCO-GNN (full)	0.81767	0.96411	0.96540	0.96555	0.96592	0.96707	0.96746
Time budget (epochs/seconds)								
Method	50/0.06	100/0.12	200/0.24	300/0.36	500/0.60	1000/1.19	2000/2.37	3000/3.56
UC Social	PI-GNN (static)	0.71087	0.91961	0.96766	0.97126	0.97284	0.97398	0.97478
	PI-GNN (warm)	0.97607	0.97654	0.97665	0.97675	0.97677	0.97670	0.97673
	DyCO-GNN (full)	0.91199	0.97913	0.97838	0.97760	0.97761	0.97708	0.97698
Time budget (epochs/seconds)								
Method	50/0.14	100/0.28	200/0.57	300/0.85	500/1.40	1000/2.80	2000/5.60	3000/8.41
DBLP	PI-GNN (static)	0.60354	0.95227	0.98754	0.98950	0.99025	0.99081	0.99113
	PI-GNN (warm)	0.99357	0.99363	0.99364	0.99364	0.99367	0.99367	0.99366
	DyCO-GNN (full)	0.99551	0.99494	0.99465	0.99437	0.99426	0.99399	0.99386

C.2 Results of the last checkpoints of DyCO-GNN on dynamic TSP

Table 7: Mean ApR on dynamic TSP. Values closer to 1 are better (\downarrow). The last checkpoint was taken. “emb”, “GNN”, and “full” refer to applying SP to the embedding layer, GNN layers, and all layers, respectively. The best result for each time budget is in bold. The first time each method surpasses the converged solution of static PI-GNN is highlighted.

Time budget (epochs/seconds)							
Method	500/0.31	1000/0.62	2000/1.24	3000/1.86	5000/3.10	10000/6.20	-
burma14	PI-GNN (static)	1.35521	1.14307	1.07890	1.06514	1.05002	1.04025
	PI-GNN (warm)	1.30116	1.29941	1.27008	1.28396	1.24094	1.16453
	DyCO-GNN (emb)	1.16825	1.15260	1.11613	1.08597	1.09302	1.08198
	DyCO-GNN (GNN)	1.13749	1.08812	1.06424	1.07396	1.05675	1.03002
	DyCO-GNN (full)	1.19695	1.15270	1.05980	1.04272	1.06671	1.08105
Time budget (epochs/seconds)							
Method	500/0.32	1000/0.64	2000/1.27	3000/1.90	5000/3.17	10000/6.36	-
ulysses22	PI-GNN (static)	1.77516	1.54757	1.29137	1.21368	1.13068	1.10295
	PI-GNN (warm)	1.18274	1.17251	1.18645	1.18424	1.18650	1.22231
	DyCO-GNN (emb)	1.21109	1.16790	1.17498	1.17131	1.15733	1.13694
	DyCO-GNN (GNN)	1.32308	1.27132	1.18273	1.14293	1.15254	1.13845
	DyCO-GNN (full)	1.36858	1.33861	1.28760	1.22112	1.16052	1.12970
Time budget (epochs/seconds)							
Method	500/0.38	1000/0.76	2000/1.51	3000/2.27	5000/3.78	10000/7.57	20000/15.16
st70	PI-GNN (static)	2.10292	2.11124	2.03993	1.94988	1.70642	1.55780
	PI-GNN (warm)	1.48778	1.49261	1.47614	1.46951	1.44118	1.43268
	DyCO-GNN (emb)	1.49505	1.49011	1.44635	1.45302	1.41491	1.38462
	DyCO-GNN (GNN)	1.65917	1.58705	1.46435	1.43776	1.44108	1.35839
	DyCO-GNN (full)	1.67305	1.68751	1.50680	1.46486	1.39795	1.37431

C.3 Snapshot-level ApRs bar plots

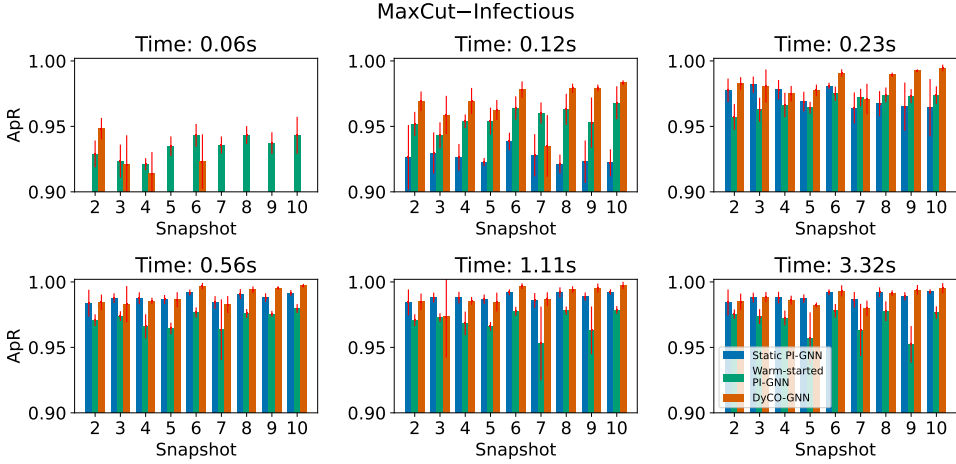


Figure 6: Snapshot-level ApRs on dynamic MaxCut instance (Infectious). All methods use GCNConv.

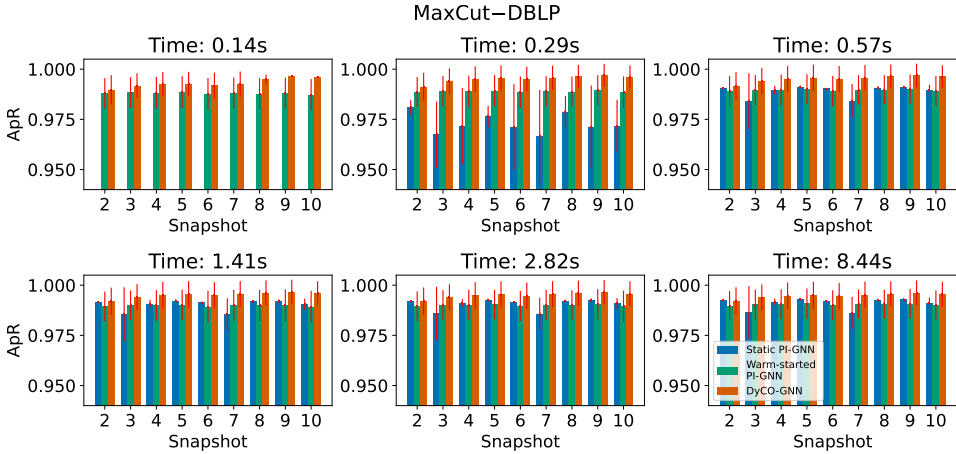


Figure 7: Snapshot-level ApRs on dynamic MaxCut instance (DBLP). All methods use GCNConv.

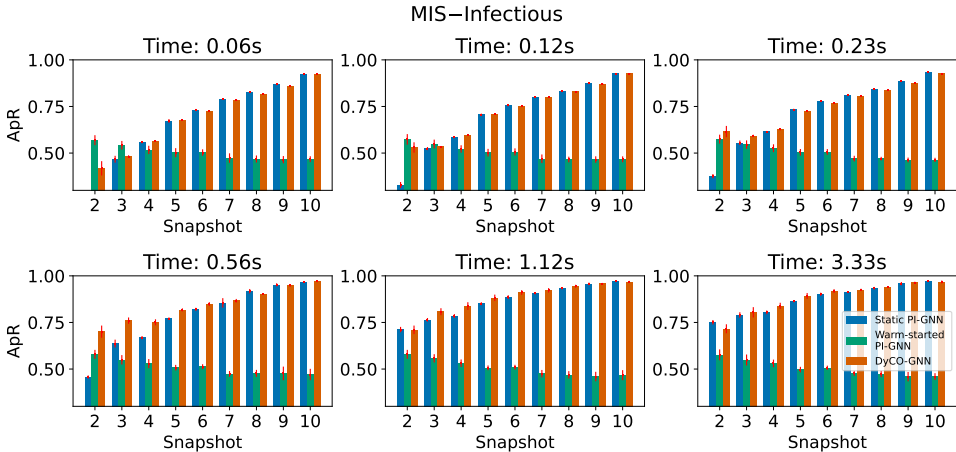


Figure 8: Snapshot-level ApRs on dynamic MIS instance (Infectious). All methods use GCNConv.

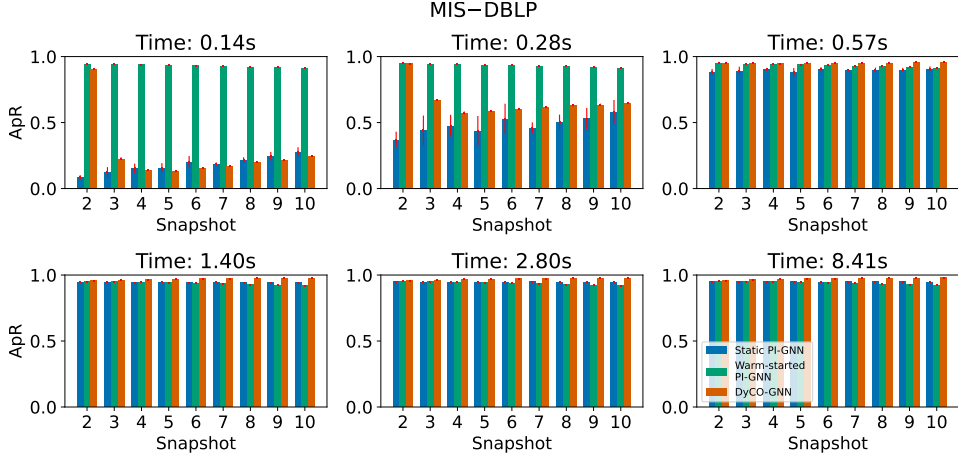


Figure 9: Snapshot-level ApRs on dynamic MIS instance (DBLP). All methods use GCNConv.

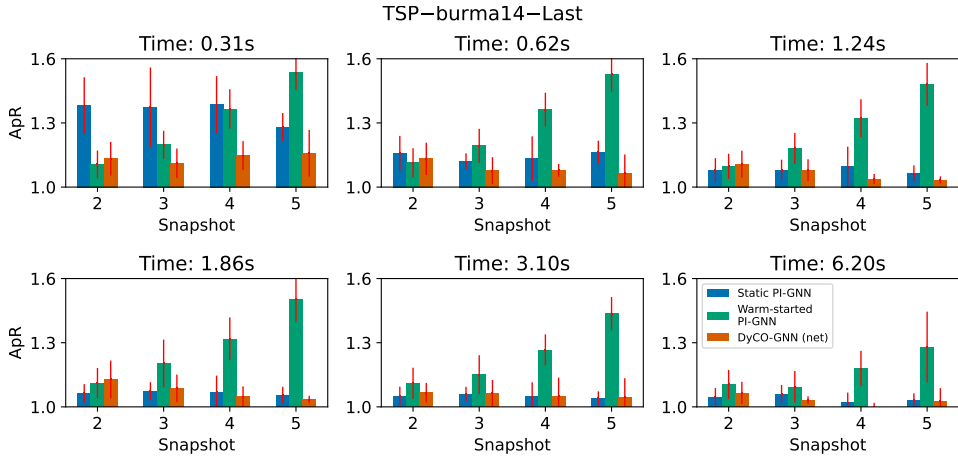


Figure 10: Snapshot-level ApRs on dynamic TSP instance (burma14). The last checkpoint was taken.

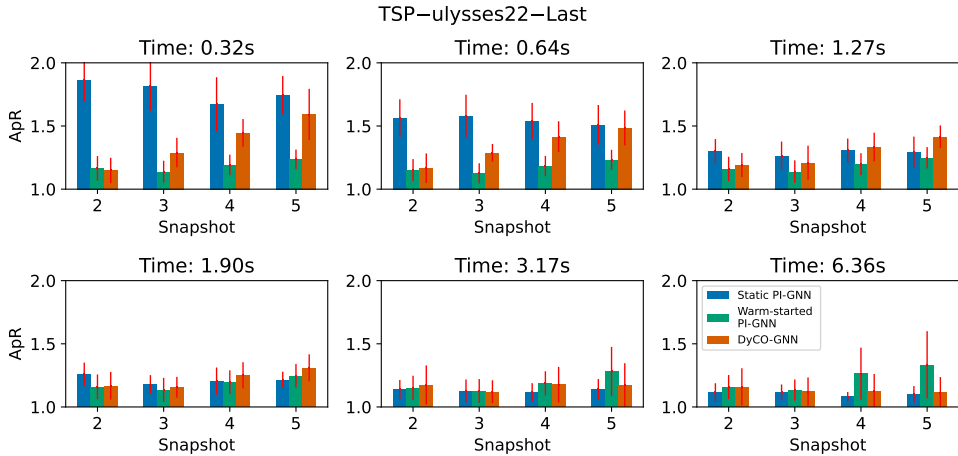


Figure 11: Snapshot-level ApRs on dynamic TSP instance (ulysses22). The last checkpoint was taken.

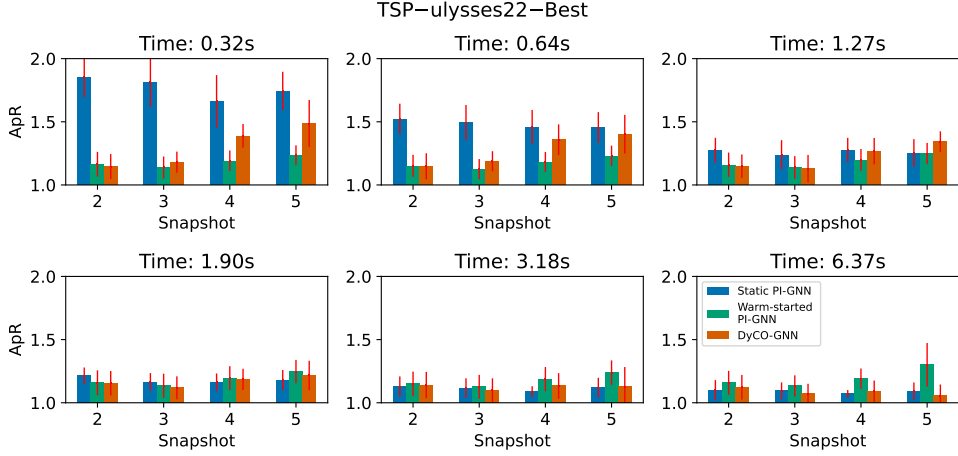


Figure 12: Snapshot-level ApRs on dynamic TSP instance (ulysses22). The best checkpoint was taken.

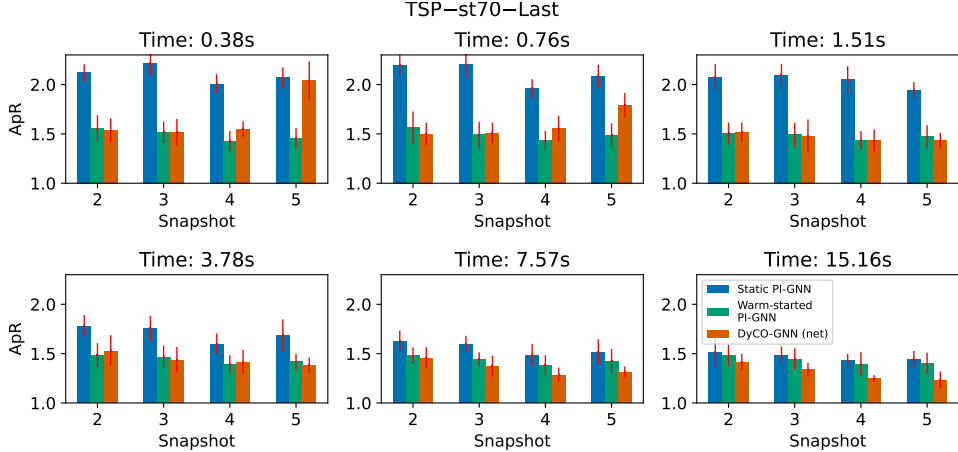


Figure 13: Snapshot-level ApRs on dynamic TSP instance (st70). The last checkpoint was taken.

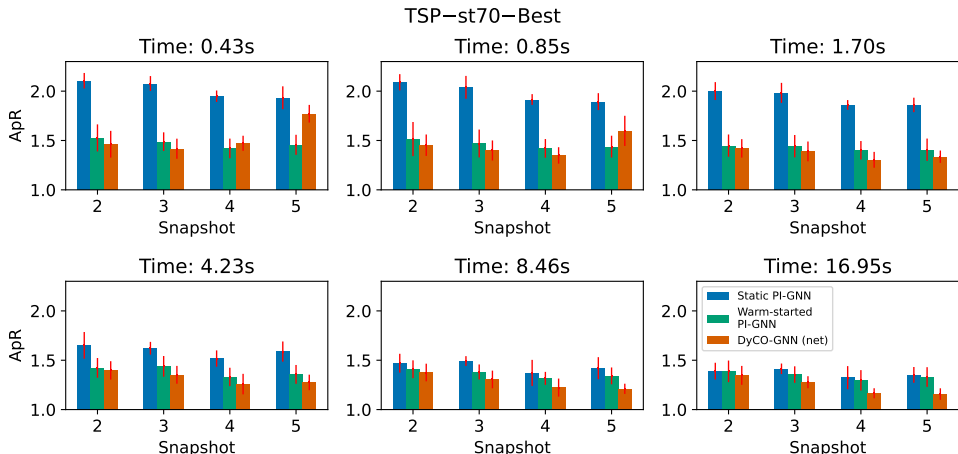


Figure 14: Snapshot-level ApRs on dynamic TSP instance (st70). The best checkpoint was taken.

D Proof and extension of Theorem 1

D.1 The Goemans-Williamson (GW) algorithm

Let $G = (V, E)$ be an unweighted graph with $|V| = n$ nodes, and let $L \in \mathbb{R}^{n \times n}$ be its Laplacian matrix. Let c^* denote the maximum achievable cut size on this graph. Our goal is to attain this maximum cut size.

Consider the following QUBO reformulation of the MaxCut problem on this graph.

$$\min \sum_{(i,j) \in E} \frac{1 - x_i x_j}{2}, \quad \text{s.t. } x_i \in \{-1, 1\}. \quad (2)$$

Goemans and Williamson [13] showed that the best approximation ratio (of at least 0.87856 times the optimal value) for the MaxCut problem can be attained by proceeding as follows. We first reformulate the above QUBO problem as the Semidefinite Program (SDP):

$$\max_X \frac{1}{4} \text{Tr}(LX), \quad \text{s.t. } X \succeq 0, \text{ diag}(X) = 1, \quad (3)$$

where $\text{Tr}(\cdot)$ denotes the trace of a matrix. Let X_{SDP}^* denote the optimal solution obtained from solving the SDP. This solution is within the feasible set $\mathcal{X} = \{X \mid X \succeq 0, \text{ diag}(X) = 1\}$; this is the set of all positive definite matrices with ones on the diagonal. Once the SDP is solved, the GW algorithm proceeds by performing a “randomized rounding” on an eigen-decomposition of the solution X_{SDP}^* to produce a binary vector representing a cut.

In more detail, consider the eigen-decomposition $X_{\text{SDP}}^* = A\Lambda A^T$ where $A \in \mathbb{R}^{n \times n}$ is an orthogonal matrix and Λ is a diagonal matrix, with the eigenvalues of X_{SDP}^* on its diagonal. Define the matrix $Y = A\Lambda^{\frac{1}{2}}$; this can be viewed as an “embedding” of the solution produced by the SDP. In it, each row Y_i corresponds to node i , which needs to be mapped to $+1$ or -1 (this will be the label of the node, which in turn will determine the two sets produced by the cut). To attain these node labels, in the rounding cut, the GW rounding algorithm samples a random vector $r \sim \mathcal{N}(0, I_n)$ (where I_n denotes the $n \times n$ identity matrix), and defines the cut to be $x_i = \text{sign}(Y_i^T r)$.

D.2 Proof of Theorem 1

Proof. First, note that the noise Z has full support on the space \mathbb{S}^n consisting of all $n \times n$ symmetric matrices, by definition. Let its distribution be denoted by ν .

Next, we show that the projection $\text{Proj}_{\mathcal{X}}$ is continuous. This is because the space \mathbb{S}^n is a finite-dimensional real Hilbert space under the Frobenius inner product $\langle A, B \rangle = \text{Tr}(AB)$. The feasible set $\mathcal{X} \subset \mathbb{S}^n$ is the intersection of the cone of positive semidefinite matrices and an affine subspace defined by linear constraints $\text{diag}(X) = 1$. Both the positive semidefinite cone and the affine subspace are closed and convex, and therefore \mathcal{X} is a closed, convex subset of a Hilbert space. By the Hilbert Projection Theorem [5, Theorem 3.12] the Euclidean projection onto any closed convex subset is continuous. Therefore, the projection function $\text{Proj}_{\mathcal{X}}$ is continuous.

Now define the function $f : \mathbb{S}^n \rightarrow \mathcal{X}$ as $f(Z) := \text{Proj}_{\mathcal{X}}(X_0 + \lambda Z)$. This function determines the distribution of \mathcal{X}_λ through the distribution of Z . Formally, let $\mu_\lambda = f_\# \nu$ be the pushforward measure on \mathcal{X} , i.e., the distribution of X_λ .

We now apply the following standard fact about pushforward measures: Let ν be a probability measure on a space Y , let $f : Y \rightarrow X$ be a measurable function, and let $\mu = f_\# \nu$ be the pushforward measure on X . Then for any measurable subset $A \subseteq X$, we have $\mu(A) = \nu(f^{-1}(A))$. In particular, if $\nu(f^{-1}(A)) > 0$, then $\mu(A) > 0$.

Back to our problem setting, note that by assumption, $\mathcal{C}_{\text{opt}} \subset \mathcal{X}$ has positive Lebesgue measure. As the measure ν of Z has full support and is absolutely continuous with respect to the Lebesgue measure on \mathbb{S}^n , and since the projection function $\text{Proj}_{\mathcal{X}}$ is continuous, the pre-image $\text{Proj}_{\mathcal{X}}^{-1}(\mathcal{C}_{\text{opt}}) \subset \mathbb{S}^n$ has positive ν -measure for some $\lambda > 0$. Therefore,

$$\mathbb{P}(R(X_\lambda) = c^*) = \mu_\lambda(C_{\text{opt}}) > 0.$$

Finally, note that by the assumption $X_0 \notin \mathcal{C}_{\text{opt}}$, we have $\mathbb{P}(R(X_0) = c^*) = 0$. This completes the proof. \square

D.3 Extension

Theorem 1 shows that the probability of finding the optimal cut strictly improves if we introduce noise pre-rounding; i.e., on a given, fixed solution of the SDP. The next corollary shows that the same result holds if we introduce noise in the initial solution of the SDP.

We use the same notation as in Theorem 1. That is, we let the feasible set of the SDP be denoted by $\mathcal{X} = \{X \mid X \succeq 0, \text{diag}(X) = 1\}$, and $\text{Proj}_{\mathcal{X}}(\cdot)$ is projection onto this feasible set \mathcal{X} . Denote the GW rounding step by $R : \{\mathcal{X}, \Omega\} \rightarrow \{0, 1, \dots, c^*\}$, where Ω is the random seed set of the cut plane and c^* is the maximum achievable cut size. We again let $\mathcal{C}_{\text{opt}} = \{X \in \mathcal{X} : \mathbb{P}_{\Omega}(R(X, \omega) = c^*) > 0\}$; this is the set of SDP solutions that have positive probability of yielding the optimal cut after the GW randomized rounding step.

Corollary 1. *Let $X_0 \in \mathcal{X}$ be the initial solution of the GW SDP. Define $X_{\lambda} := \text{Proj}_{\mathcal{X}}[X_0 + \lambda Z]$, where $\lambda \in \mathbb{R}_{\geq 0}$, and Z is a symmetric random matrix sampled from the Gaussian Orthogonal Ensemble. Let $\Pi_{\text{SDP}}(X)$ denote the SDP solver starting from a feasible solution X , and assume that it is locally continuous. Assume that the set \mathcal{C}_{opt} has positive Lebesgue measure in \mathcal{X} , that $\Pi(X_0) \notin \mathcal{C}_{\text{opt}}$. Then, there exists a $\lambda > 0$ such that*

$$\mathbb{P}_{\Omega, Z}(R(\Pi(X_{\lambda}), \omega) = c^*) > \mathbb{P}_{\Omega}(R(\Pi(X_0), \omega) = c^*) = 0.$$

The proof is straightforward: given the assumption that the SDP solver $\Pi(\cdot)$ is locally continuous, that means that small perturbations of the initial SDP solution X_0 map to perturbations of the solution $\Pi(X_0)$. Consequently, the results of Theorem 1 are applicable. We note that SDP solvers for solving MaxCut, such as interior-point methods, are locally continuous under mild assumptions; e.g. [43].

E Broader impacts

The DyCO-GNN framework introduces an efficient, UL approach for solving DCO problems without requiring offline training or labeled datasets. DyCO-GNN’s ability to efficiently adapt to evolving problem instance snapshots without optimization from scratch or external supervision enables more rapid and resource-efficient optimization in time-sensitive environments such as supply chain management, transportation systems, disaster response, and real-time network routing.

The potential societal benefits of DyCO-GNN are significant. By avoiding heavy training pipelines, DyCO-GNN can operate in low-resource settings and adapt on-the-fly to changes in problem structure, promoting computational sustainability. Furthermore, the ability to dynamically update solutions has implications for reducing operational delays and improving responsiveness in real-world systems.

However, the framework may also pose ethical and societal risks. There is the risk of dual-use. Also, the objective functions optimized by DyCO-GNN may not capture critical social or ethical constraints, such as fairness or safety, which could lead to unintended consequences if applied to human-centered systems. To mitigate these risks, we encourage future work on integrating human-in-the-loop constraints and ethical guardrails directly into dynamic optimization objectives.